



Enhanced activity and durability of the oxygen reduction catalysts supported on the surface expanded tubular-type carbon nanofiber

Jiyoung Kim^{a,b}, Ui-Su Im^{a,b}, Dong-Hyun Peck^{a,b}, Seong-Ho Yoon^c, Ho Seok Park^d, Doo-Hwan Jung^{a,b,*}

^a Advanced Energy and Technology, University of Science and Technology (UST), Yuseong-gu, Daejeon, 305-333, Republic of Korea

^b New and Renewable Energy Research Division, Korea Institute of Energy Research (KIER), Yuseong-gu, Daejeon, 305-343, Republic of Korea

^c Institute for Materials Chemistry and Engineering, Kyushu University, Kasuga, Fukuoka, 816-8580, Japan

^d School of Chemical Engineering, Sungkyunkwan University (SKKU), Jangan-gu, Suwon, 440-746, Republic of Korea

ARTICLE INFO

Article history:

Received 29 December 2016

Received in revised form 30 April 2017

Accepted 31 May 2017

Available online 1 June 2017

Keywords:

Carbon nanofiber

Surface modification

Oxygen reduction reaction

Fuel cell catalyst

ABSTRACT

Tubular type carbon nanofibers (TCNFs) are prepared and used as a catalyst support material for a cathode electrode of low temperature fuel cells through structural modification. The pristine TCNF is treated by graphitization and makes partially torn-tube shape through the surface expansion by rapid thermal treatment of the oxidized graphitized TCNF. Physical properties of the TCNF group are examined, and it is confirmed that the unique ripped texture along fiber axis with graphitic structure is obtained by the surface expansion. Platinum catalysts supported on these TCNF group are prepared and evaluated. Electrochemical properties are examined via cyclic voltammograms and polarization curves for oxygen reduction reaction activity. The platinum catalyst on the surface expanded TCNF has the enhanced activity at initial and the stable performance even after accelerated durability test due to their unique structure.

© 2017 Elsevier B.V. All rights reserved.

1. Introduction

Carbon nanofibers (CNFs) have attracted great attention as unique nanomaterials having a potential for industrial applications such as functional composites, electrochemical electrodes, semiconductor devices, electron emitters, catalysts and catalyst supports [1–6]. A number of studies on selective synthesis and structural analysis have been performed to attain uniform and controlled structure of the CNFs [7–9]. The most important factor to determine the properties of the CNF is a stacking configuration of graphene layer. The CNFs are classified into three groups as platelet (PCNF), herringbone (HCNF) and tubular (TCNF) types [10]. The graphene layers of the PCNF are stacked in the direction of perpendicular to the growth axis, so the PCNF has relatively large diameter and plenty of exposure of edge sites. The HCNF has tilted graphene layers based on the structure of the PCNF, and it leads to thinner diameter and larger specific surface area than the PCNF. The TCNF (is also known as CNT), which the graphene

layers locate the same direction of fiber axis, forms the exposure of stable basal planes on the carbon surface. The TCNF has been used as a catalyst support material due to relatively high surface area, excellent electronic conductivity, and high chemical stability. Many studies about the synthesis and application of the TCNF as a support material of platinum electro-catalyst for fuel cells, especially focusing on cathode electrode with high durability were conducted [11–13]. As mentioned above, the TCNF dominantly wrapped by stable basal plane typically has a good electrical conductivity and a robust structure caused by higher graphitic degree. Without the surface modification, however, lack of sufficient binding sites for anchoring precursor metal ions or metal nanoparticles is happened. This usually leads to poor dispersion and agglomeration of metal nanoparticles. It has a significant impact on the catalyst activity and durability. Therefore, the introduction of proper functionality onto the TCNF or structural modification is the essential ingredient for future applications.

In this presenting study, we first prepared the iron-nickel (Fe-Ni) binary catalyst and synthesized the TCNFs over the Fe-Ni catalyst from a mixture of carbon monoxide (CO) and hydrogen gases. The TCNFs were heat-treated at the temperature of graphitization to retain their robust original structure against further harsh procedure. The graphitized TCNFs were conducted additional surface modification through the expansion of graphene layer induced

* Corresponding author at: Advanced Energy and Technology, University of Science and Technology (UST), Yuseong-gu, Daejeon, 305-333, Republic of Korea / New and Renewable Energy Research Division, Korea Institute of Energy Research (KIER), Yuseong-gu, Daejeon, 305-343, Republic of Korea.

E-mail address: doohwan@kier.re.kr (D.-H. Jung).

by strong oxidation and rapid heat treatment [14]. Subsequently, pristine TCNF and modified TCNFs were used as support materials for Pt/C. Electro-catalytic activities such as electrochemical surface area and oxygen reduction reaction are analyzed based on the study of the surface modification of the TCNFs. Also, we tried to evaluate the possibility as the promising support material by carrying out the accelerated durability test.

2. Experimental

2.1. Fe-Ni catalyst for TCNF

A Fe-Ni (weight ratio of Fe:Ni = 6:4) catalyst was prepared using iron nitrate ($\text{Fe}(\text{NO}_3)_3 \cdot 9\text{H}_2\text{O}$), nickel nitrate ($\text{Ni}(\text{NO}_3)_2 \cdot 6\text{H}_2\text{O}$) and ammonium hydrogen carbonate (NH_4HCO_3). Prescribed amount of Fe and Ni agent were dissolved in 300 mL of distilled water and heated at 90 °C with stirring. When the metal nitrates were perfectly dissolved, NH_4HCO_3 of 3 times of metal weight was slowly added into the mixture with vigorous stirring. The mixture was left the rest for stabilization at room temperature for 8 h, and then filtered and washed with distilled water of 4 L. The second step to prepare the Fe-Ni catalyst with nano-sized structure to enhance the catalytic activity was conducted by further heat-treatment. Pristine Fe-Ni catalyst was treated at 400 °C in air flow for 4 h to induce the slight oxidation and form the nanostructure. The reactor was cooled down under inert atmosphere and the Fe-Ni catalyst was heated for reduction at 500 °C in flow of hydrogen for 20 h. When the reactor was cooled down and attempted aging at 35 °C in air for 1 h, the prepared Fe-Ni catalysts were collected.

2.2. Preparation and modification of the TCNF

The TCNF was synthesized using a middle-scale vertical furnace with the capacity of 5 g per day. The Fe-Ni catalyst (0.1 g) was spread on the reaction quartz bed assisted by an acetone and then the reactor was purged with helium gas. The furnace heated up to designed temperature during 2 h. When the temperature of furnace reached synthesis condition, supplied gas was changed to helium and hydrogen mixture (volume ratio 4:1 = He:H₂) for reduction of Fe-Ni catalyst for 30 min. After an atmosphere was replaced with helium for 30 min, the TCNF was synthesized from carbon monoxide and hydrogen gases (volume ratio of 1:1) over Fe-Ni catalyst for 2 h. After that, the gas mixture was re-changed with helium and hydrogen for stabilization of the TCNF for 30 min and cooled down under inert helium gas. The amount of the total reaction gas was fixed to 1 L/min. The TCNF was treated with 10 wt% hydrochloric acid (HCl) solution twice over 24 h to remove the metallic catalysts. Finally, the sample was sufficiently washed with distilled water and dried overnight at 80 °C.

Further treatment in order to obtain substantial structure called graphitization was conducted in extremely high temperature. The graphitization treatment was performed at 2800 °C in flow of argon for 10 min. The TCNF processed this graphitization referred as the G-TCNF.

A surface expansion of the G-TCNF was done through both of strong oxidation and followed rapid thermal treatment [15]. Three gram of the G-TCNF was immersed in high concentrated H₂SO₄ of 98 wt% for 12 h with stirring, and then 9 g of KMnO₄ was slowly added in an ice bath. The temperature of solution was carefully paid attention not to exceed 55 °C. When the KMnO₄ was dissolved completely, the temperature raised up to 70 °C and stirred for 1 h. Distilled ice of 300 g and 35 wt% H₂O₂ solution of 90 mL were poured into the mixture for quenching, and then the reaction was finished with vigorous stirring for 3 h. The oxidized G-TCNF slurry was separated and collected using a centrifuge with 4800 rpm, and

washed with 1 M HCl solution. The oxidized G-TCNF was completely prepared by washing with distilled water, filtration and dryness overnight. A surface expansion of the oxidized G-TCNF was conducted by rapid thermal treatment. The oxidized G-TCNF was placed onto a reaction bed in helium purged horizontal tube furnace. The temperature was rapidly elevated to 300 °C in a rate of 30 °C/min, and then the elevate speed was changed in 5 °C/min up to 900 °C. The heat-treatment at 900 °C was kept going for 3 h. During the rapid thermal treatment, the formation of water droplets was discovered due to the elimination of oxidative components in the carbon structure. After the reaction was finished and cooled down, the sample was collected and named as the EG-TCNF. All carbon samples were treated by 1 M HNO₃ solution for 24 h to create the oxygen function groups on the surface.

2.3. Preparation of Pt catalyst supported on the TCNF group

The target loading weight of Pt and the amount of Pt/C were set as 40 wt% and 0.5 g. Pt/C was synthesized by a pH controlled polyol method using ethylene glycol (EG). Pt reagent was previously mixed with 3 times of EG. After the carbons were put into EG of 200 mL with sonication for 30 min, Pt/EG and 1 M NaOH/EG solution to transfer an alkaline. The mixture was heated at 150 °C for 3 h with reflux system, and then cooled down and stabilized for 12 h. One mole of H₂SO₄/EG was poured into the solution to adjust to the neutral pH. In sequence, the reactor was heated up to 120 °C for 3 h and stabilized at room temperature for 24 h. These Pt/C catalysts by the polyol method were finished with filtration and cleaning with distilled water.

2.4. Characterizations

Morphologies of synthesized and modified TCNF group were observed via a scanning electron microscope (SEM, JSM-6700F, JEOL) and a transmission electron microscope (TEM, JEM-2100F, JEOL). Oxidative resistance profiles of the TCNF group were confirmed using thermogravimetric analysis (TG, STA409PC, NETZSCH). Structural properties such as specific surface area and porosity were inspected from nitrogen adsorption-desorption profile at liquid nitrogen temperature and further calculation using BET and BJH formula. X-ray diffraction profiles were obtained using a Rigaku instrument (RINT-Ultima III) with a Cu K α radiation. Raman spectroscopy was performed on the Dimension-P1 Raman system with 530 nm laser wavelength.

Pt loading content of the Pt/C catalysts was found out from the amount of residual in the TG. Crystallite size of the Pt particle on the TCNF group was calculated by the Scherrer equation from the Pt (220) peak at 68° of 2-theta in the XRD pattern. The deposition of Pt particles on the TCNF group was confirmed using a field emission TEM (Talos F200X). We selected 100-particle samples from the TEM images to reveal the particle size distribution. Electrochemical activities of each catalyst were evaluated using conventional three electrode system. Mirror-polished glassy carbon with a diameter of 5 mm was used as the working electrode. A Pt coil and a silver/silver chloride electrode (SSCE) were used as the counter and the reference electrode, respectively. All of the electrode potentials were converted with references of the reversible hydrogen electrode (RHE). A catalyst slurry was prepared by blending the catalysts of 10 mg and 5 wt% Nafion solution of 57.2 μL in distilled water of 7.5 mL and isopropyl alcohol of 2.5 mL with vigorous stirring and sonicated for 20 min in an ice bath. Ten micro-liter of the catalyst slurry was pipetted onto the working electrode. The amount of loaded Pt on working electrode was calculated from the dry matter weight of 30 times of 10 μL catalyst slurry referring TG data. Before the electrochemical measurement for catalytic activities, the cleaning of prepared working electrode was performed

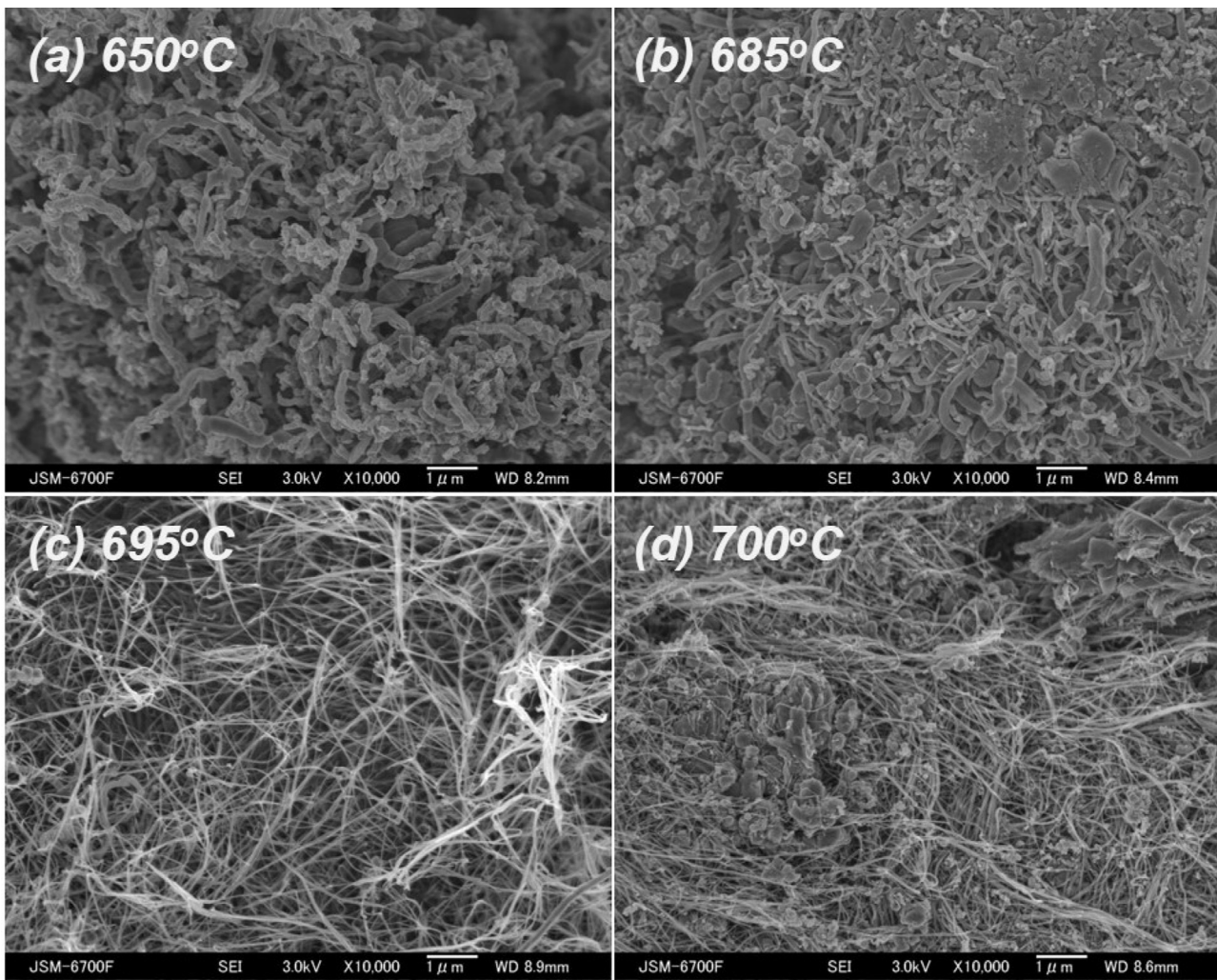


Fig. 1. Scanning electron microscope (SEM) images of temperature-sensitive carbon nanofibers (CNFs) synthesized at (a) 650 °C, (b) 685 °C, (c) 695 °C, and (d) 700 °C.

via the potential cycling from 0.025 to 1.2 V vs. RHE at a scan rate of 500 mV/s for 100 cycles. Cyclic voltammograms (CVs) were obtained with the potential sweep between 0.025 and 1.0 V vs. RHE at a scan rate of 20 mV/s in a nitrogen purged 0.1 M HClO₄ electrolyte. Hydrogen adsorption areas of the CV curves were used to calculate the electrochemical surface area (ECA). The oxygen reduction reaction (ORR) activities were measured in an oxygen purged 0.1 M HClO₄ electrolyte with the linear potential sweep from 0.025 to 1.0 V vs. RHE at a scan rate of 20 mV/s. The working electrode was rotated at 1600 rpm during the ORR measurement. Electrochemical impedance spectroscopy in an oxygen purged electrolyte was obtained to measure the solution resistance (R_{soln}) for the ORR kinetic currents. Accelerated durability tests (ADT) were carried out CVs in a range of 0.6–1.2 V vs. RHE at 100 mV/s in an oxygen saturated electrolyte for 5000 cycles. After 100, 200, 500, 1000, 3000, and 5000 cycles, the performance changes were discovered with the CV and ORR measurements described above. All electrochemical measurements were carried out using a Bio-Logic VSP.

3. Results and discussion

3.1. Physical analysis of the TCNF group

Fig. 1 shows the SEM images of the CNFs in accordance with synthesis temperature in the range of 650–700 °C. In Fig. 1(a), the platelet type CNF was synthesized in relatively low temperature

nearby 650 °C from the decomposition of CO gases over the Fe-Ni catalyst. The PCNF showed a relatively large diameter and joint shape according to growth direction. As the synthesis temperature increased, the PCNF partially became thin and smooth shape like tubular type CNF. Fig. 1(c) at 695 °C showed the well-developed TCNFs with long and thin fiber. Over the 700 °C, the destruction of fibrous form was occurred by high temperature, the carbon files like a form of rock were observed by improper thermal decomposition of hydrocarbon containing gas. Here, the PCNF and TCNF were able to be prepared over the Fe-Ni catalyst and the structural feature of the CNFs was very sensitive to the synthesis temperature. In the followed experiments, the TCNF at 695 °C was used as a matrix material.

The TEM images of the TCNF group are presented in Fig. 2. There were obviously different morphologies in the pristine TCNF, the G-TCNF and the EG-TCNF. The TCNF had well-defined tubular structure with a blank at the core part. The basal plane of graphene layer was exposed in parallel direction with the axis of fiber growth. As the graphitization treatment at 2800 °C, the unique structure of the graphitized CNFs appeared. The graphene layer also developed more clearly, so the whole shape of the G-TCNF looked like a bamboo-type CNF with unusual joint to disconnect the middle length of tubes. The TEM images of the EG-TCNF by the strong oxidation and rapid heat treatment informed that the tubular and fibrous shape slightly disappeared by the tear of partial surface along the fiber axis direction as shown in Fig. 2(c). Though the

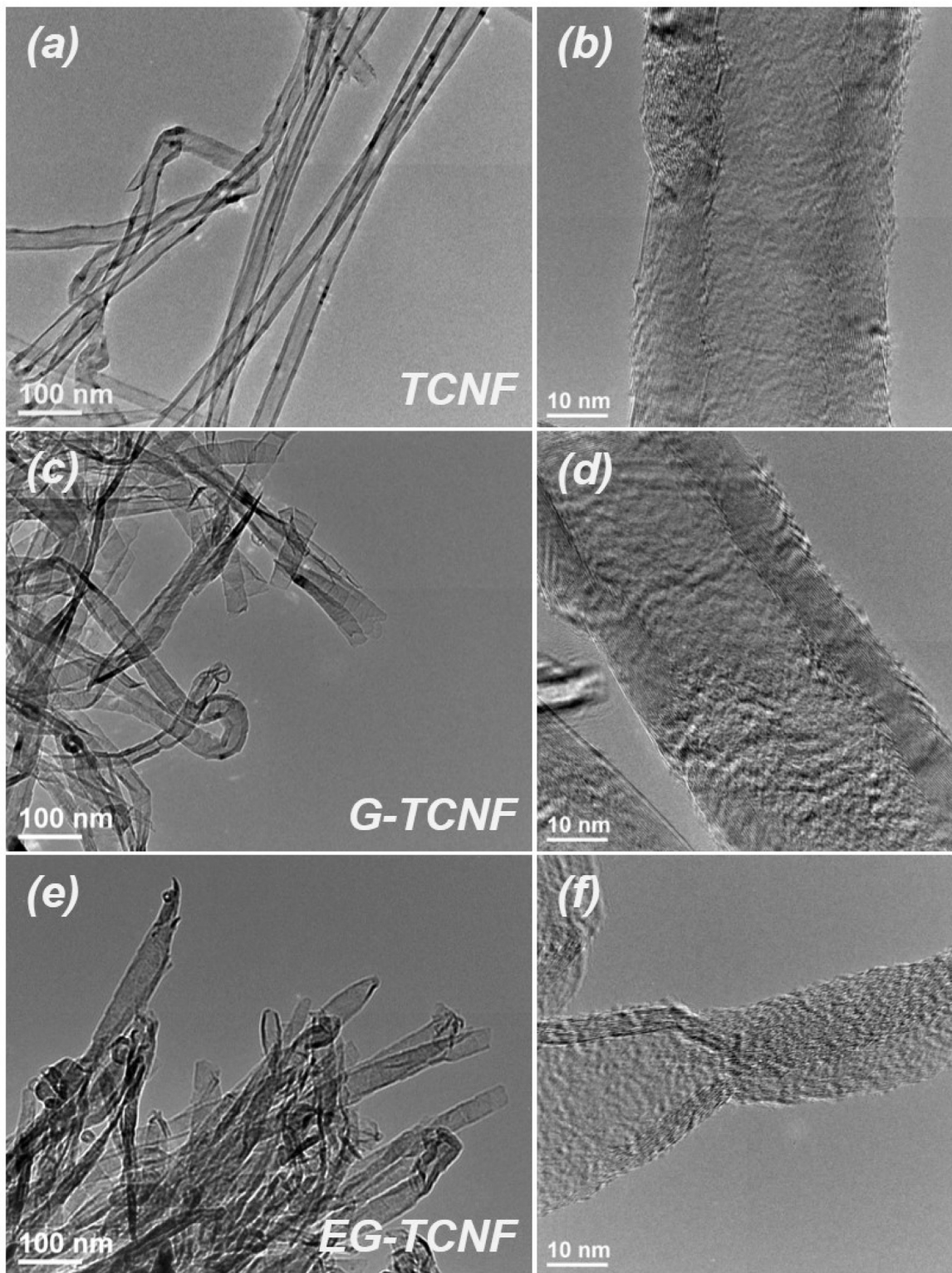


Fig. 2. Transmission electron microscope (TEM) photographs for comparison of the CNF structure. (a,b) Pristine tubular CNF (TCNF). (c,d) Graphitized TCNF (G-TCNF). (e,f) Surface expanded G-TCNF (EG-TCNF).

pristine TCNF had well-developed fibrous shape and had a relatively high resistance to oxidation than the PCNF or the HCNF, the most part of tubular structure was destroyed to the expanded form like the EG-TCNF. Even, after the graphitization of the TCNF, the fibrous structure could not be maintained by harsh surface modification, and the surface expansion was successfully turned up.

Nitrogen adsorption-desorption isotherm profiles and pore distributions by BJH method of the TCNF group are examined in Fig. 3. The specific surface areas by the BET calculation were 98, 54 and 153 m²/g for the TCNF, G-TCNF and EG-TCNF, respectively. After the graphitization, the specific surface area was reduced by a half and mesoporous parts were almost disappeared. The specific surface

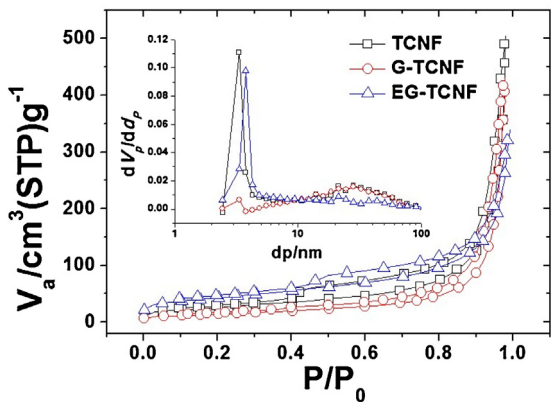


Fig. 3. Nitrogen sorption isotherm profiles of the CNFs and their pore size distributions by Barrett-Joyner-Halenda (BJH) method (inset figure).

area and porosity were returned to increase more than the original one through the surface expansion process. The specific surface area of the EG-TCNF increased three times higher than that of the G-TCNF, and that was a 50% increase of the pristine TCNF. The amount of mesopores of the EG-TCNF were not significantly increased than the pristine TCNF, but the pore size was slightly positively shifted in Fig. 3 inner one. Mesopore regions of the TCNF were eliminated via the graphitization, while those were revived by the surface expansion process. It is considered that mesopores of the TCNF were contributed by the defects on the surface or empty core parts at the tip of the fibers. In case of the EG-TCNF, there may be substantial mesopores which were contributed by the unzipped parts in the direction of fiber axis through the surface expansion. Also, the specific surface area of the EG-TCNF significantly increased by the exposure of the inner tube to outside since there is no formation of micropores. These results agree with the TEM observations. XRD patterns of the TCNF group are presented in Fig. 4. The XRD patterns were revealed that the graphitization degree of the TCNF and the G-TCNF exhibited a high value as d_{002} of 0.339 nm with a very sharp peak. The stacking height L_c of the TCNF and the G-TCNF were 9.7 and 13.4 nm, respectively. However, the EG-TCNF had higher value of d_{002} of 0.342 nm because the widen graphene layers by the strong oxidation were not fully recovered by further rapid heat-treatment, and there were structural changes. The broaden peak was observed in the EG-TCNF and the L_c was significantly reduced to 3.7 nm. The changes of Raman spectroscopy according to the surface modification procedure of the TCNF group is shown in Fig. 5. Two main

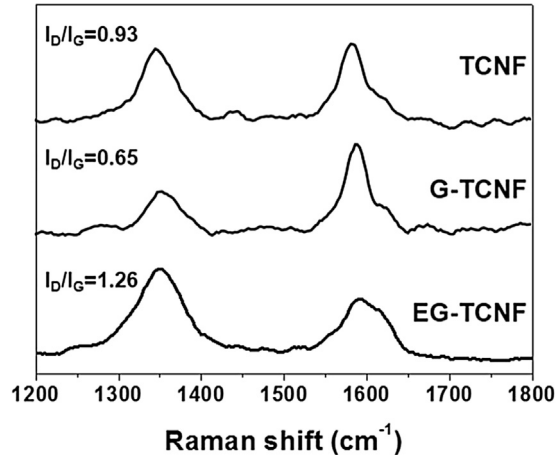


Fig. 5. Raman spectra of the TCNF, G-TCNF and EG-TCNF corresponding with I_D/I_G value.

peaks, which estimate the interlayer structure of the TCNF group, were separated at 1348 cm^{-1} of the D-band and at 1586 cm^{-1} of the G-band. The D-band represents a dis-ordered graphene layer, and the G-band is known as the graphite or tangential C–C band. The degree of conjugation disruption can be determined from the intensity ratio (I_D/I_G) values of the D-band and the G-band. The Raman results also shows the agreement with the above surface analysis for the experimental procedures. The TCNF had a value of 0.93 of the ratio, indicating that it has a considerable degree of graphitization. When the TCNF was heat-treated at the extremely high temperature, the carbon atoms in the structure could be rearranged and the Raman intensity ratio was significantly reduced through this graphitization. However, the I_D/I_G value increased to 1.26 via the surface structure change of the EG-TCNF. And this implied that the EG-TCNF has sufficient defect density for the deposition of catalytic metal particle due to the cracking of graphite C–C bond or exposure of edge plane by the surface modification.

The weight loss of the TCNF group by the combustion using TG analysis is shown in Fig. 6. The decomposition of carbon molecules in the TCNF was started at nearby 500°C , but graphitized carbon like the G-TCNF began at 700°C . The oxidation resistance of the TCNF significantly increased through the graphitization process. In case of the EG-TCNF, any particular behavior of entire profiles is not detected excepting earlier beginning of the weight loss at 600°C . The EG-TCNF had a considerably reduced oxidation resistance than the G-TCNF due to the harsh post-treatment and the increased surface area by the surface expansion. The EG-TCNF also had lower graphitization degree and stacking height as the results of XRD and

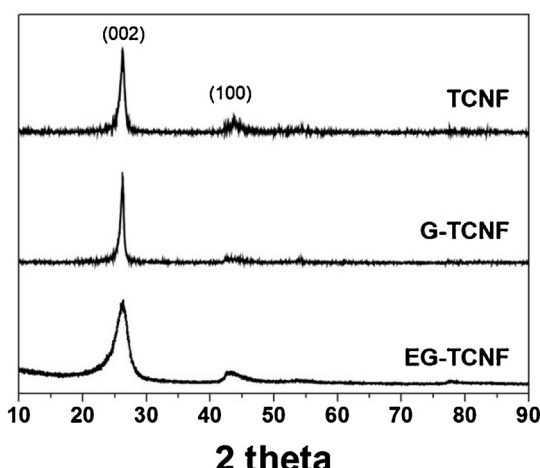


Fig. 4. X-ray diffraction (XRD) profiles of the TCNF group.

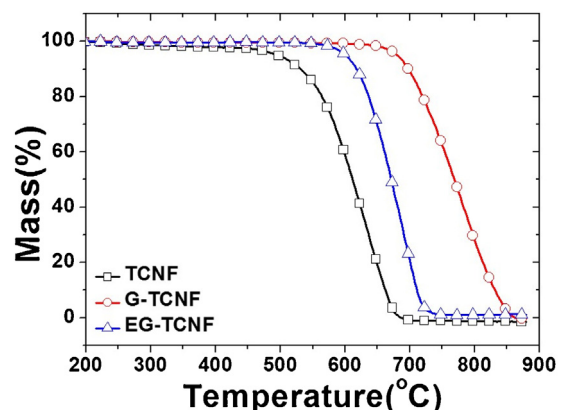


Fig. 6. Thermogravimetric analysis of the TCNF, G-TCNF, and EG-TCNF.

Table 1

Physical characteristics of Pt catalysts supported on the TCNF group.

Pt/C Support material	Pt content (%)	Avg. Pt crystallite size (nm)	
		XRD	TEM
TCNF	41.4	3.6	3.3
G-TCNF	40.8	2.1	2.8
EG-TCNF	40.5	1.7	2.5

Raman. However, the unit structure seemed to be had a sufficient oxidation resistance by the graphitization process, so an improved durability of the EG-TCNF is expected rather than the pristine TCNF.

3.2. Characterization of Pt catalysts on the TCNF group

Pt content estimated from the residual of the TG data at 800 °C is summarized in Table 1. Targeted 40 wt% Pt/C catalysts were properly synthesized using pH controlled polyol method. The mean crystallite sizes of the Pt from Pt (220) peak of the XRD pattern by the Scherrer formula and from TEM images of Pt catalysts are also summarized in Table 1. Fig. 7 shows TEM images of the Pt/C catalyst and the particle size distribution from it. Since the basal plane of the graphene layer occupied the most surface of the TCNF, the anchoring sites to attach the Pt particles were insufficient even though the introduction of oxygen functional group by HNO₃ treatment. Therefore, the Pt particles were not dispersed well shown in Fig. 7(a). The larger particles of 4 nm or more were found due to the partial agglomeration of particles during the deposition process as seen in the particle size distribution. The G-TCNF had a unique surface morphology due to the graphitization process as shown in Fig. 2. The G-TCNF had a bamboo type morphology in overall shape, and the intermediate joints seen as a disconnection part seemed to be an edge plane. In Fig. 7(b), these bamboo joints acted as an anchoring site, so the Pt particles seemed to be deposited in a certain line. The average particle size of the Pt/G-TCNF was 2.8 nm, which was smaller than that of Pt/TCNF, but some large particles were found. Using the EG-TCNF as a support material, it had the smallest average particle size of 2.5 nm and the ideal narrow particle size distribution. In the TEM image, although there were empty places where platinum particles were not applied partially, the uniform distribution of the Pt/EG-TCNF would be induce a higher catalytic activity.

3.3. Electrochemical performance of the Pt/TCNF group

Fig. 8(a) and (b) indicate the CVs and linear curves for the ORR of the Pt catalysts on the TCNF group. When the different carbon supports are applied on the working electrode, its surface may vary depending on the structural characteristics of the carbon supports or the degree of catalyst dispersion in the slurry. Although the limiting current density of all samples did not exactly match in the ORR experiment, we make efforts to present the reasonable result. The electrochemical surface areas (ECAs) calculated from the hydrogen adsorption area of the CVs in Fig. 8(a) are summarized in Table 2. The ECA of 41.5 m²/g for the Pt/EG-TCNF was slightly higher than that of Pt/TCNF of 40.8 m²/g. On the other hand, the Pt/G-TCNF had a low active surface area of 29.4 m²/g. The Pt/G-TCNF had smaller and well dispersed Pt particles than the Pt/TCNF as shown in Fig. 7, but the electrochemical performance was not excellent. The ECA was significantly reduced by the graphitization, and was increased twice due to the changes in morphology through the surface expansion such as the Pt/EG-TCNF. As reported in many research results, it is difficult to expect high performance when the graphitized carbon was used as a support material because of the reduction of surface area and the problem of particle dispersion and so on. Fig. 8(b) show the initial ORR performance. The ORR curves were handled with the compensation processing of both iR_{soln} and background correction [16]. The ORR also showed similar trends for Pt/TCNF and Pt/EG-TCNF like as the CVs. Mass activity and specific activity, which were additionally corrected by Koutecký-Levich equation for kinetic currents, of the ORR at 0.9 V vs. RHE are summarized in Table 2. The Pt/EG-TCNF showed the highest performance on the kinetic dominant current area with less overpotential as a cathode side. In the 0.8–0.4 V vs. RHE where the diffusion controlled region, however, the Pt/TCNF showed predominant performance and reached the limiting current density more rapidly. The Pt/G-TCNF exhibited a low ORR activity of less than half of other catalysts similar to the result of ECA. The graphitization group of Pt/G-TCNF and Pt/EG-TCNF displayed a similar slope, and it seemed to be due to the effect of graphitization on the unit structure of the TCNF, even though further analysis and deep consideration is required. It was confirmed that the reduced activity due to the graphitization such as the Pt/G-TCNF could be recovered to slightly higher performance than the pristine Pt/TCNF due to the surface expansion such as the Pt/EG-TCNF. In addition, the graphitic unit structure of the EG-TCNF is expected to remain as the TG result, which provides higher durability.

The profiles of the accelerated durability test (ADT) for evaluating the stability of each Pt/C catalyst are indicated in Fig. 9. The 0.1 M HClO₄ electrolyte was purged with oxygen during the ADT to

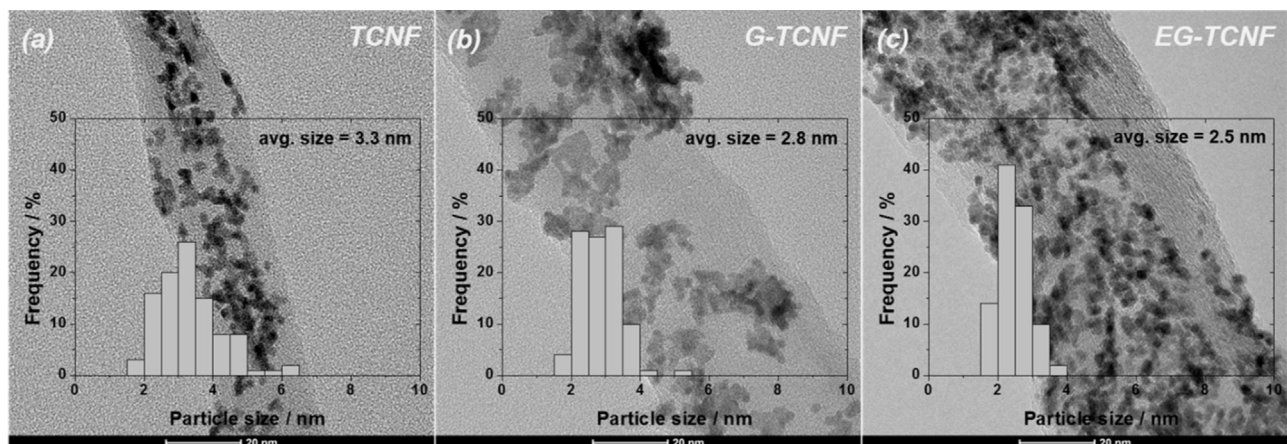


Fig. 7. TEM images with Pt particles on the TCNF group. Inset figure show the particle size distribution.

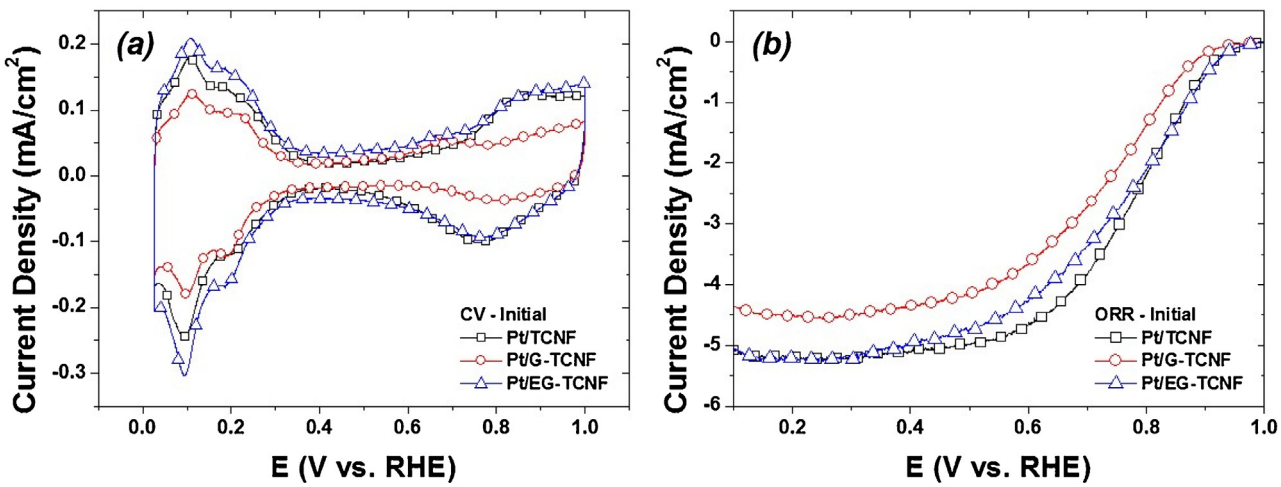


Fig. 8. Comparisons of initial (a) cyclic voltammograms and (b) polarization curves for oxygen reduction reaction.

Table 2

Initial catalytic activity of electrochemical surface area and oxygen reduction reaction of the Pt/C group. Mass activity and specific activity are compensated with electrolyte solution resistance, background current and oxygen diffusion using K-L equation.

Pt/C Support material	ECA ($\text{m}^2/\text{g}_{\text{Pt}}$)	ORR activity @ 0.9 V vs. RHE	
		Mass activity (mA/mg _{Pt})	Specific activity ($\mu\text{A}/\text{cm}^2_{\text{-Pt}}$)
TCNF	40.8	27.7	67.9
G-TCNF	29.4	10.3	35.0
EG-TCNF	41.5	29.8	71.8

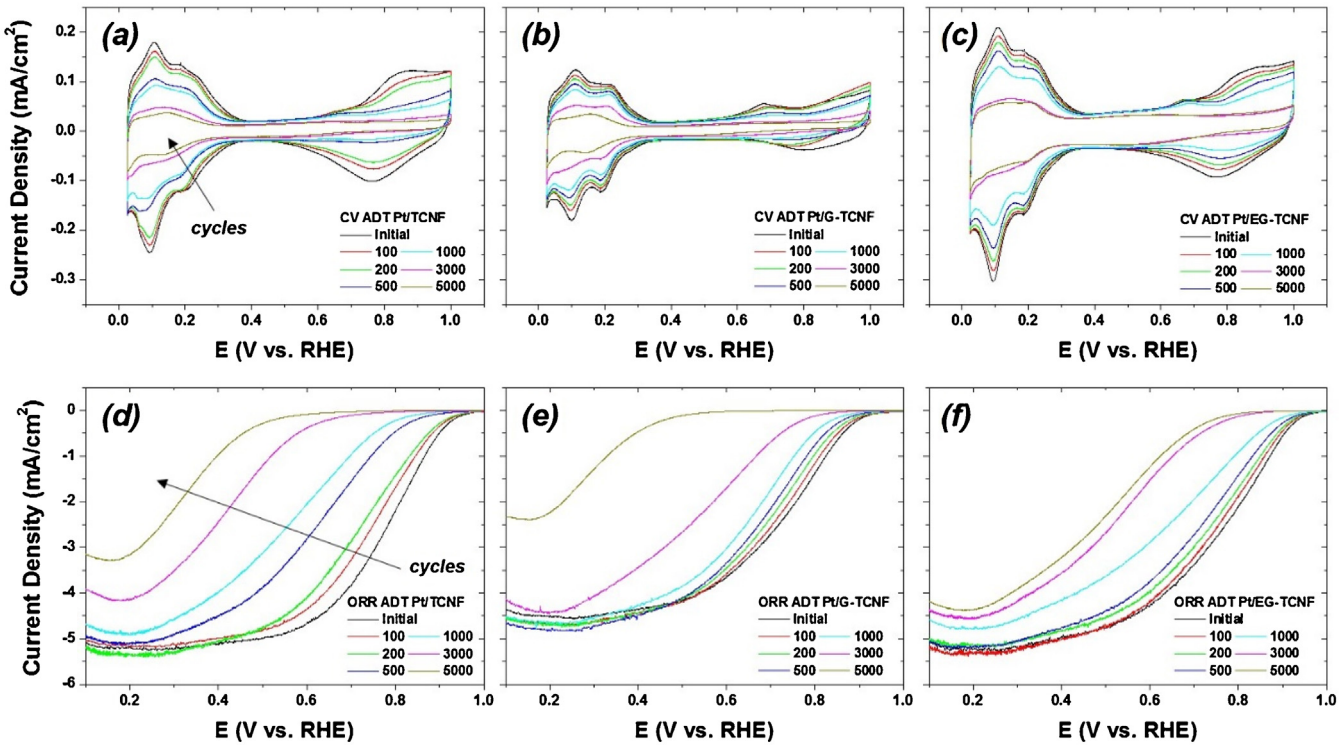


Fig. 9. Profiles of CVs and ORR curves of (a,d) Pt/TCNF, (b,e) Pt/G-TCNF and (c,f) Pt/EG-TCNF according to the accelerated durability test (ADT).

examine the durability under the same condition as the cathode of fuel cells. Fig. 9(a)-(c) are CV results after the ADT for the Pt/TCNF, Pt/G-TCNF and Pt/EG-TCNF, respectively. As the cycling proceed, it can be estimated that the hydrogen adsorption area obviously decreases. In particular, the area between the 1000–3000 cycles

was sharply reduced, and the current peak for the facet of Pt particle also became weakening. The changes of the ORR curves according to the ADT are shown in Fig. 9(d)–(f). The ORR curves shifted in a negative direction and the limiting current density value also decreased as the cycle progresses. For the Pt/TCNF, the activity for

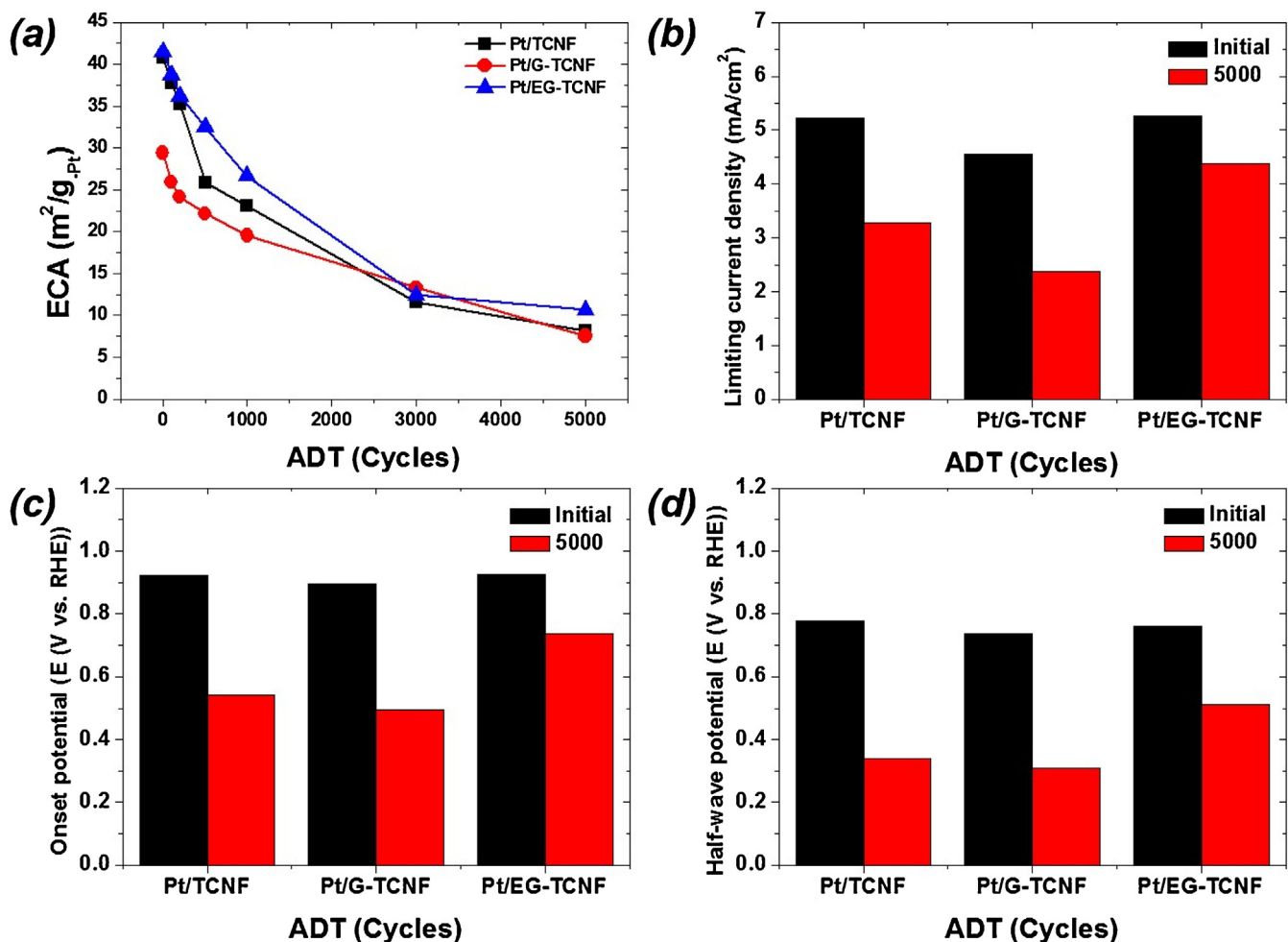


Fig. 10. Performance comparisons between the initial and after ADT for (a) electrochemical surface area (ECA), (b) limiting current density, (c) onset potential and (d) half-wave potential.

ORR was gradually decreased according to the ADT. However, the Pt/G-TCNF and the Pt/EG-TCNF were resisted to the initial performance degradation. Although the Pt/G-TCNF did not present significant reduction in the ORR activity until 1000 cycles, after then the drastic decline was occurred. The Pt/G-TCNF also had a limitation to the low initial ORR performance. On the other hand, the Pt/EG-TCNF maintained outstanding durability over the last 5000 cycles with high initial performance.

The major parameters of performance changes according to the ADT are compared in Fig. 10. Fig. 10 (a) shows the variation of electrochemical surface area calculated from the CVs. The Pt/EG-TCNF kept a high active area over the entire cycle, although the performance of all catalysts seemed to be overlapped at 3000th cycle. Other factors such as (b) limiting current density, (c) onset potential and (d) half-wave potential at the initial and 5000th cycle are compared. The reasons for the decrease in the limiting current density are able to be considered as the dissociation of Pt particles and agglomeration by re-deposition. It is also conceivable that the catalyst could be detached from the working electrode due to the support carbon corrosion. The onset potential was calculated as the potential indicating a current density which is 5% of the limiting current density. The half-wave potential was obtained by the same method as the onset potential except 50% of the limiting current density. The positively high potential value means that the catalyst has high catalytic activity. The Pt/EG-TCNF had the highest initial activity as shown in Table 2 and stable performance after the ADT. The EG-TCNF induced the unique surface characteristics such as

dis-ordered graphene layer texture and edge plane exposure by the surface modification, which may improve the stronger interaction with Pt particles. Therefore, well-dispersed platinum deposition could be achieved and better electrochemical performance was obtained. Additionally, the Pt/EG-TCNF had a high oxidation resistance since they had graphitized basic unit structures as shown in Fig. 6, and it matched well with our ADT results. Meanwhile, the merits of slurry production for manufacturing a membrane electrode assembly (MEA), it did not experiment in this case unfortunately, can be considered. Because twisted form of long fibers was transformed into two-dimensional stacking structure with short and platy group through the surface expansion. From these results, the Pt catalyst supported on the EG-TCNF is expected to be a good selection as a cathode electrode material for low temperature fuel cells.

4. Conclusions

We synthesized and modified the tubular type carbon nanofibers (TCNFs) to apply for a catalyst support material of a cathode electrode for low temperature fuel cells. The pristine TCNF was prepared over the Fe-Ni catalyst via chemical vapor deposition of CO gas. To achieve the superior catalytic performance and durability, the graphitized TCNF (G-TCNF) was reformed to the expansion of structure (EG-TCNF) by the strong oxidation and following rapid thermal treatment. The EG-TCNF with the basic structure of graphitized TCNF possess the unique surface structure with partially

torn-tube shape. Platinum catalysts using the TCNF group were prepared using pH controlled polyol method using ethylene glycol. The electrochemical surface area (ECA) and the ORR activity of the Pt/C catalysts were remarkably influenced by the carbon support material. The ECA of Pt/TCNF, Pt/G-TCNF and Pt/EG-TCNF is 40.8, 29.4 and 41.5 m²/g. Not only the kinetic ORR activity at 0.9 V vs. RHE but also the durability result appears the highest value at the Pt/EG-TCNF. Since the EG-TCNF with split surface along the fiber axis has the graphitized unit-structure and unique morphology with easy access of reactants, it could provide the enhanced performance and durability.

Acknowledgements

This work was conducted under the framework of the Research and Development Program of the Korea Institute of Energy Research (KIER) (B6-2420-03) in Republic of Korea. This work was also supported by the Innopolis commercialization of technology development project funded by the INNOPOLIS Foundation in Republic of Korea.

References

- [1] K.P. De Jong, J.W. Geus, Carbon nanofibers: catalytic synthesis and applications, *Catal. Rev. Sci. Eng.* 42 (2000) 481–510.
- [2] P. Kichambare, J. Kumar, S. Rodrigues, B. Kumar, Electrochemical performance of highly mesoporous nitrogen doped carbon cathode in lithium-oxygen batteries, *J. Power Sources* 196 (2011) 3310–3316.
- [3] R.H. Baughman, A.A. Zakhidov, W.A. de Heer, Carbon nanotubes – the route toward applications, *Science* 297 (2002) 787–792.
- [4] C. Kim, K.S. Yang, Electrochemical properties of carbon nanofiber web as an electrode for supercapacitor prepared by electrospinning, *Appl. Phys. Lett.* 83 (2003) 1216.
- [5] Y.J. Wang, N. Zhao, B. Fang, H. Li, X.T. Bi, H. Wang, Carbon-supported Pt-based alloy electrocatalysts for the oxygen reduction reaction in polymer electrolyte membrane fuel cells: particle size, shape, and composition manipulation and their impact to activity, *Chem. Rev.* 115 (2015) 3433–3467.
- [6] D.B. Thakur, R.M. Tiggelaar, J.G.E. Gardeniers, L. Lefferts, K. Seshan, Silicon based microreactors for catalytic reduction in aqueous phase: use of carbon nanofiber supported palladium catalyst, *Chem. Eng. J.* 227 (2013) 128–136.
- [7] R.T.K. Baker, M.S. Kim, A. Chambers, C. Park, The relationship between metal particle morphology and the structural characteristics of carbon deposits, *Stud. Surf. Sci. Catal.* 111 (1997) 99–109.
- [8] W.W. Pang, S. Lim, Y.Z. Zhang, S.H. Yoon, I. Mochida, The bimetallic effects of catalysts on the syntheses of thin carbon nanofibers, *J. Phys. Chem. C* 112 (2008) 10050–10060.
- [9] S. Lim, S.H. Yoon, I. Mochida, J. Chi, Surface modification of carbon nanofiber with high degree of graphitization, *J. Phys. Chem. B* 108 (2004) 1533–1536.
- [10] A. Tanaka, S.H. Yoon, I. Mochida, Preparation of highly crystalline nanofibers on Fe and Fe-Ni catalysts with a variety of graphene plane alignments, *Carbon* 42 (2004) 591–597.
- [11] W. Li, C. Liang, J. Qiu, W. Zhou, H. Han, Z. Wei, G. Sun, Q. Xin, Carbon nanotubes as support for cathode catalyst of a direct methanol fuel cell, *Carbon* 40 (2002) 787–803.
- [12] C. Wang, M. Waje, X. Wang, J.M. Tang, R.C. Haddon, Yushan, Proton exchange membrane fuel cells with carbon nanotube based electrodes, *Nano Lett.* 4 (2004) 345–348.
- [13] T. Matsumoto, T. Komatsu, K. Arai, T. Yamazaki, M. Kijima, H. Shimizu, Y. Takasawa, J. Nakamura, Reduction of Pt usage in fuel cell electrocatalysts with carbon nanotube electrodes, *Chem. Commun.* 7 (2004) 840–841.
- [14] D. Long, W. Li, J. Miyawaki, W. Qiao, L. Ling, I. Mochida, S.H. Yoon, Meso-channel development in graphitic carbon nanofibers with various structures, *Chem. Mater.* 23 (2011) 4141–4148.
- [15] W.S. Hummers Jr., R.E. Offeman, Preparation of graphitic oxide, *J. Am. Chem. Soc.* 80 (1958) 1339.
- [16] K. Shinozaki, J.W. Zack, R.M. Richards, B.S. Pivovar, S.S. Kocha, Oxygen reduction reaction measurements on platinum electrocatalysts utilizing rotating disk electrode technique – I. Impact of impurities, measurement protocols and applied corrections, *J. Electrochem. Soc.* 162 (2015) 1144–1158.